Scientific paper

Novel Benzimidazole-Based Compounds as Antimicrobials: Synthesis, Molecular Docking, Molecular Dynamics and *in silico* ADME Profile Studies

Elif Yeşilçayır,[1] İsmail Çelik,[2] Hasan Tahsin Şen,[1,3] Suna Sibel Gürpınar,[4] Müjde Eryılmaz,[4] Gülgün Ayhan-Kılcıgil[1]*

[1] *Ankara University, Faculty of Pharmacy, Department of Pharmaceutical Chemistry, Ankara, Turkey*

[2] *Erciyes University, Faculty of Pharmacy, Department of Pharmaceutical Chemistry, Kayseri, Turkey*

[3] *Lokman Hekim University, Faculty of Pharmacy, Department of Pharmaceutical Chemistry, Ankara, Turkey*

[4] *Ankara University, Faculty of Pharmacy, Department of Pharmaceutical Microbiology, Ankara, Turkey*

* *Corresponding author: E-mail: kilcigil@pharmacy.ankara.edu.tr*

Received: 12-03-2021

Abstract

Some novel benzimidazole derivatives were synthesized and their antimicrobial activities were evaluated. Compounds **3a** and **3b** exhibited excellent antibacterial activity with MIC values <4 μg/mL against *Staphylococcus aureus* ATCC 29213 (MSSA) and *Staphylococcus aureus* ATCC 43300 (MRSA). Molecular docking analyzes of compounds with MIC values of 16 μg/mL and below against gram-positive bacteria and fungi were performed using FabH (β-ketoacyl-acyl carrier protein synthase III) as bacterial protein and CYP51 (sterol 14α-demethylase) as the fungal target protein. According to the molecular docking analysis, it was calculated that sufficient protein-ligand interaction energy was liberated between the compounds **2f**, **3a**, **3b**, **3e** and **3h** and the antibacterial target protein FabH and strong interactions were formed between **2f** and **3h** and the antifungal target protein. According to RMSD, RMSF and MMPBSA measurements obtained from molecular dynamics, it is understood that compounds **3a** and **3b** maintain protein-ligand stability *in silico* physiological conditions.

Keywords: Benzimidazole, antimicrobial activity, molecular docking, molecular dynamics

1. Introduction

Microbes are disease agents that cause death. Today, the transmission of diseases to large masses has become an increasing threat to human health. Antibiotic resistance remains at dangerously high levels around the world. This situation leads to new resistance mechanisms and spreads the resistance globally, making it difficult to treat infectious diseases. Furthermore, antimicrobial resistance is recognized globally as one of the greatest health threats; thus, the discovery of alternative antibacterial agents to address antimicrobial resistance is a priority target. Effective treatment of infections and complete elimination of antimicrobial resistance can be achieved with the use of new antimicrobial compounds.

It is well known that benzimidazoles have antibacterial,[1] antimicrobial,[2–5] and antifungal[6] activities. Furthermore, several benzimidazoles show promising pharmacological activities such as antioxidant,[7–9] anticancer,[10] anti-inflammatory,[11] antiprotozoal,[12] antiviral,[13] antidiabetic,[14] antihypertensive,[15] antimycobacterial,[16] and antithrombin,[17] as well as tubulin[18] and dipeptidyl peptidase III[19] inhibitors.

In view of extending our previous studies on the synthesis and bioactivity of benzimidazole derivatives,[20–21] we synthesized a series of 4-(1*H*-benzimidazol-2-yl)-6-arylpyrimidin-2-amines. Moreover, we also evaluated their antibacterial and antifungal activities and carried out molecular docking and molecular dynamics simulation studies.

2. Experimental

2. 1. Chemistry

All reagents and solvents were used as purchased, without further purification. The reactions were moni-

tored by thin-layer chromatography (TLC) analysis using silica gel plates (Kieselgel 60F254, E. Merck). Column chromatography was performed on Silica Gel 60 M (0.040–0.063 mm, E. Merck). Melting points were determined on a Büchi B540 capillary melting point apparatus and are uncorrected. The ^{1}H and ^{13}C NMR spectra were recorded on a Varian 400 MHz and Bruker 500 MHz FT spectrometer in DMSO-d_6, shift values are given in parts per million relative to tetramethylsilane as internal reference and coupling constants (*J*) are reported in Hertz. Mass spectra were taken on a Waters Micromass ZQ connected with Waters Alliance HPLC, using ESI+ method, with the C-18 column. Elemental analyses were performed by Leco CHNS-932 analyzer.

2. 1. 1. Synthesis of 2-(α-Hydroxyethyl) benzimidazole

o-Phenylenediamine (0. 025 mol) and lactic acid (3.2 mL) were refluxed for 3 h. The reaction mixture was cooled and made alkaline with 10% aq. NaOH. The crude product obtained was dissolved in boiling water and decolorized with activated charcoal. The mixture was filtered and washed with cold water.[22–24]

2. 1. 2. Synthesis of 2-Acetylbenzimidazole

To the solution of $K_2Cr_2O_7$ (0.15 mol) in H_2SO_4 (25%, 10 mL) was added dropwise a solution of 2-(α-hydroxyethyl)benzimidazole (0.01 mol) in 5% H_2SO_4 (5 mL) while stirring at room temperature over a period of 20 min. The reaction mixture was stirred at room temperature for 2 h. The reaction mixture was neutralized with aqueous NH_3 solution (1:1) and the precipitated solid was filtered, washed with water, dried and recrystallized from ethyl acetate.[23,24]

2. 1. 3. Synthesis of 1-(1*H*-Benzimidazol-2-yl)-3-aryl-prop-2-en-1-ones 2a–h

2-Acetylbenzimidazole (0.01 mol) and aromatic aldehydes (0.01 mol) were mixed with ethanol (20 mL) and added 60% aq. KOH (5 mL) at 0 °C and the mixture were stirred at room temperature for 4 h. After completion of the reaction (controlling TLC, chloroform:hexane 1/3), the reaction mixture was poured into ice-cold water and neutralized with dilute HCl solution. The solid formed was filtered, washed, dried and recrystallized from ethanol.[23,24]

(*E*)-1-(1*H*-Benzimidazol-2-yl)-3-(3-bromo-4-fluorophenyl)prop-2-en-1-one (2a)

Yield 73%; mp 214 °C. ^{1}H NMR (400 MHz, DMSO-d_6) δ 7.3–7.5 (m, 3H, Ar-H), 7.56 (d, 1H, *Jo* = 8 Hz, Ar-H), 7.83–7.95 (m, 3H, Ar-H and C*H*=CH), 8.09 (d, 1H, J_{trans} = 16 Hz, CH=C*H*), 8.25–8.26 (m, 1H, Ar-H), 13.51 (s, 1H, NH); ^{13}C NMR (100 MHz, DMSO-d_6) δ 108.9 (d, *J* = 21.4 Hz), 112.94, 117.4 (d, *J* = 22.9 Hz), 121.7, 112.7, 123.2, 125.8, 130.3 (d, *J* = 8.45 Hz), 132.8 (d, *J* = 3.11 Hz), 134.0, 134.8, 141.6, 143.0, 148.8, 159 (d, *J* = 250.05 Hz), 180.8; MS (ESI+) *m/z* 345.40 (M+H), 347.39 (M+H+2). Anal. Calcd for $C_{10}H_{10}BrFN_2O$: C, 55.68; H, 2.92; N, 8.12. Found: C, 55.83; H, 3.19; N, 7.88.

(*E*)-1-(1*H*-Benzimidazol-2-yl)-3-(naphthalen-2-yl) prop-2-en-1-one (2b)

Yield 34%; mp 225 °C. ^{1}H NMR (500 MHz, DMSO-d_6) δ 7.35–7.37 (m, 1H, Ar-H), 7.41–7.44 (m, 1H, Ar-H), 7.90 (d, 1H, *Jo* = 8.15 Hz, Ar-H), 7.98–8.06 (m, 4H, Ar-H), 8.15 (d, 1H, J_{trans} = 16 Hz, C*H*=CH), 8.26 (d, 1H, J_{trans} = 16 Hz, CH=C*H*), 8.43 (s, 1H, Ar-H), 13.52 (s, 1H, NH); ^{13}C NMR (125 MHz, DMSO-d_6) δ 113.39, 121.63, 122.32, 123.71, 124.76, 126.28, 127.39, 128.23, 129.24, 129.28, 131.42, 132.39, 133.45, 134.62, 135.29, 143.54, 144.80, 181.39; MS (ESI+) *m/z* 299.60 (M+H). Anal. Calcd for $C_{20}H_{14}N_2O$: C, 80.52; H, 4.73; N, 9.39. Found: C, 80.23; H, 4.41; N, 9.80.

(*E*)-1-(1*H*-Benzimidazol-2-yl)-3-(naphthalen-1-yl)prop-2-en-1-one (2c)

Yield 44%; mp 216 °C. ^{1}H NMR (500 MHz, DMSO-d_6) δ 7.35–7.41 (m, 2H, Ar-H), 7.35–7.43 (m, 2H, Ar-H), 7.61–7.70 (m, 4H, Ar-H), 7.90 (d, 1H, *J* = 7.6 Hz, Ar-H), 8.04 (d, 1H, *J* = 8.30 Hz, Ar-H), 8.10 (d, 1H, *J* = 8.10 Hz, Ar-H), 8.18–8.23 (2H, Ar-H and C*H*=CH), 8.36 (d, 1H, *J* = 8.45 Hz, Ar-H), 8.82 (d, 1H, J_{trans} = 15.85 Hz, CH=C*H*), 13.57 (brs, 1H, NH); ^{13}C NMR (125 MHz, DMSO-d_6) δ 113.41, 121.68, 123.50, 123.70, 124.57, 126.28, 126.35, 126.93, 127.91, 129.36, 131.51, 131.70, 131.83, 133.91, 135.31, 140.85, 143.57, 149.44, 181.29; MS (ESI+) *m/z* 299.55 (M+H). Anal. Calcd for $C_{20}H_{14}N_2O$: C, 80.52; H, 4.73; N, 9.39. Found: C, 80.33; H, 4.92; N, 9.15.

(*E*)-1-(1*H*-Benzimidazol-2-yl)-3-(4-bromophenyl)prop-2-en-1-one (2d)

Yield 80%; mp 229 °C. ^{1}H NMR (400 MHz, DMSO-d_6) δ 4.82 and 5.46 (td, 1H, *J* = 7.6 Hz, Ar-H), 7.21–7.47 (m, 5H, Ar-H), 7.67–7.85 (m, 3H, Ar-H), 7.94 and 8.14 (d, 1H, J_{trans} = 16 Hz, CH=CH), 13.18 and 13.53 (s, 1H, NH); ^{13}C NMR (100 MHz, DMSO-d_6) δ 119.81, 122.27, 124.52, 129.86, 130.84, 130.86, 132.13, 133.57, 138.21, 142.87, 147.76, 148.90, 180.88, 192.09; MS (ESI+) *m/z* 327.51 (M+H), 329.49 (M+H+2). Anal. Calcd for $C_{16}H_{11}BrN_2O$: C, 58.74; H, 3.39; N, 8.56. Found: C, 59.07; H, 3.72; N, 8.24.

(*E*)-1-(1*H*-Benzimidazol-2-yl)-3-phenylprop-2-en-1-one (2e)

Yield 71%; mp 224 °C (lit.[23] 162–164 °C). ^{1}H NMR (400 MHz, DMSO-d_6) δ 7.36–7.38 (m, 2H, Ar-H), 7.47–7.49 (m, 3H, Ar-H), 7.70–7.89 (m, 4H, Ar-H), 7.98 (d, 1H, J_{trans} = 16 Hz, CH=CH), 8.13 (d, 1H, J_{trans} = 16 Hz, CH=CH), 13.51 (brs, 1H, NH); ^{13}C NMR (100 MHz, DM-

SO-d_6) δ 121.53, 128.94, 129.14, 131.11, 134.30, 144.25, 148.99, 180.96; MS (ESI+) *m/z* 249.47 (M+H). Anal. Calcd for $C_{16}H_{12}N_2O$: C, 77.40; H, 4.87; N, 11.28. Found: C, 77.65; H, 5.21; N, 10.91.

(*E*)-1-(1*H*-Benzimidazol-2-yl)-3-(2-fluorophenyl)prop-2-en-1-one (2f)

Yield 13%; mp 212 °C. ^{1}H NMR (400 MHz, DMSO-d_6) δ 7.29–7.38 (m, 4H, Ar-H), 7.52–7.55 (m, 2H, Ar-H), 7.86 (d, 1H, *J* = 6.8 Hz, Ar-H), 7.97–8.01 (m, 2H, Ar-H and CH=CH), 8.18 (d, 1H, J_{trans} = 16.4 Hz, CH=CH), 13.52 (brs, 1H, NH); ^{13}C NMR (100 MHz, DMSO-d_6) δ 113.36, 116.75 (d, *J* = 21.3 Hz), 121.70, 123.47 (d, *J* = 11.5 Hz), 123.71, 124.49 (d, *J* = 6.1 Hz), 125.73, 126.36, 130.66, 133.52 (d, *J* = 8.4 Hz), 135.29, 136.60, 143.49, 149.23, 160.66 (d, *J* = 250.7 Hz), 181.33 (d, *J* = 3.8Hz); MS (ESI+) *m/z* 267.49 (M+H). Anal. Calcd for $C_{16}H_{11}FN_2O$: C, 72.17; H, 4.16; N, 10.52. Found: C, 71.79; H, 4.49; N, 10.86.

(*E*)-1-(1*H*-Benzimidazol-2-yl)-3-[4-(benzyloxy)phenyl] prop-2-en-1-one (2g)

Yield 45%; mp 240 °C. ^{1}H NMR (400 MHz, DMSO-d_6) δ 5.2 (s, 2H, CH2), 7.13 (d, 2H, *J* = 8.8 Hz, Ar-H), 7.34–7.49 (m, 7H, Ar-H), 7.6 (brs, 1H), 7.84–8.03 (m, 5H, Ar-H and CH=CH); ^{13}C NMR (100 MHz, DMSO-d_6) δ 69.88, 115.73, 115.92, 119.54, 127.59, 128.24, 128.32, 128.51, 128.94, 128.95, 131.42, 132.34, 137.07, 144.69, 149.62, 161.32, 181.27; MS (ESI+) *m/z* 355.54 (M+H). Anal. Calcd for $C_{23}H_{18}N_2O_2$: C, 77.95; H, 5.12; N, 7.90. Found: C, 77.52; H, 4.79; N, 8.28.

(*E*)-1-(1*H*-Benzimidazol-2-yl)-3-(thiophen-2-yl)prop-2-en-1-one (2h)

Yield 67%; mp 224 °C. ^{1}H NMR (400 MHz, DMSO-d_6) δ 7.22–7.24 (m,1H, Ar-H), 7.31–7.42 (m, 2H, Ar-H), 7.73 (d, 1H, *J* = 3.6 Hz, Ar-H), 7.80 (d, 1H, J_{trans} = 15.6 Hz, CH=CH), 7.85–7.88 (m, 2H, Ar-H), 8.15 (d, 1H, J_{trans} = 16 Hz, CH=CH); ^{13}C NMR (100 MHz, DMSO-d_6) δ 180.35, 148.94, 143.51, 139.69, 137.01, 135.26, 134.27, 131.17, 129.09, 126.23, 123.68, 121.62, 119.86, 113.31; MS (ESI+) *m/z* 255.30 (M+H). Anal. Calcd for $C_{14}H_{10}N_2OS$: C, 66.12; H, 3.96; N, 11.02; S, 12.61. Found: C, 65.83; H, 3.50; N, 11.45; S, 12.97.

2. 1. 4. Synthesis of 4-(1*H*-Benzimidazol-2-yl)-6-arylpyrimidin-2-amines 3a–h

0.81 mmol arylidene benzimidazole **2a–h** was added at 0 °C to the mixture of 1.08 mmol (103.4 mg) guanidine hydrochloride and 2.16 mmol (51.94 mg) sodium hydride in 2.7 mL DMF, stirred for 1 h at room temperature and for another 3 h at 100 °C. The reaction mixture was poured onto the crushed ice and pH adjusted to 7 with dilute HCl. The precipitate was filtered and purified by column chromatography using chloroform/methanol, 10/0.5 as the eluent.[25]

4-(1*H*-Benzimidazol-2-yl)-6-(3-bromo-4-fluorophenyl) pyrimidin-2-amine (3a)

Yield 26%; mp 130 °C. ^{1}H NMR (500 MHz, DMSO-d_6) δ 6.91 (brs, 2H, NH_2), 7.24–7.32 (m, 2H, Ar-H), 7.55 (td, 1H, *J* = 8.65 Hz, 8.60 Hz, Ar-H), 7.61 (d, 1H, *Jo* = 7.85 Hz, Ar-H), 7.75 (d, 1H, *Jo* = 7.9 Hz, Ar-H), 7.98 (s, 1H, pyrimidine H-5), 8.25–8.28 (m, 1H, Ar-H), 8.54 (dd, 1H, *Jo* = 6.8 Hz, *Jm* = 2.6 Hz, Ar-H), 13.04 (s, 1H, NH); ^{13}C NMR (125 MHz, DMSO-d_6) δ 102.93, 109.10–109.27 (d, *J* = 21.26 Hz), 112.96, 117.56–117.73 (d, *J* = 22.46 Hz), 120.03, 122.77–124.29 (d, *J* = 190.65 Hz), 128.92–128.98 (d, *J* = 7.96 Hz), 132.39, 135.24–135.31–135.34 (2×d, *J* = 9.34 Hz, 3.44 Hz), 144.13, 149.85, 158.00, 158.25, 161.24, 163.00, 164.20; MS (ESI+) *m/z* 384.48 (M+H), 386.50 (M+H+2). Anal. Calcd for $C_{17}H_{11}BrFN_5$: C, 43.90; H, 2.60; N, 15.06. Found: C, 44.39; H, 2.98; N, 14.85.

4-(1*H*-Benzimidazol-2-yl)-6-(naphthalen-2-yl)pyrimidin-2-amine (3b)

Yiel 29%; mp 231 °C. ^{1}H NMR (500 MHz, DMSO-d_6) δ 6.87 (brs, 2H, NH_2), 7.25–7.33 (m, 2H, Ar-H), 7.60–7.64 (m, 3H, Ar-H), 7.77 (d, 1H, *Jo* = 7.9 Hz, Ar-H), 8.00–8.02 (m, H, Ar-H), 8.09 (d, 1H, *Jo* = 8.75 Hz, Ar-H), 8.15–8.17 (m, 2H, Ar-H), 8.34 (dd, *Jo* = 8.65 Hz, *Jm* = 1.75 Hz, Ar-H), 8.83 (s, 1H, pyrimidine H-5), 13.05 (s, 1H, NH); ^{13}C NMR (125 MHz, DMSO-d_6) δ 103.28, 112.97, 120.01, 122.73, 124.20, 124.41, 127.15, 127.45, 127.91, 128.06, 128.81, 129.47, 133.33, 134.59, 134.64, 135.28, 144.18, 150.08, 157.68, 164.35, 165.41; MS (ESI+) *m/z* 338.58 (M+H). Anal. Calcd for $C_{21}H_{15}N_5$: C, 74.76; H, 4.48; N, 20.76. Found: C, 74.29; H, 4.75; N, 20.38.

4-(1*H*-Benzimidazol-2-yl)-6-(naphthalen-1-yl)pyrimidin-2-amine (3c)

Yield 26%; mp 152 °C. ^{1}H NMR (500 MHz, DMSO-d_6) δ 6.91 (brs, 2H, NH_2), 7.24 (td, 1H, *J* = 8.15 Hz, 1.15 Hz, Ar-H), 7.30 (td, 1H, *J* = 8.15 Hz, 1.15 Hz, Ar-H), 7.57–7.67 (m, 5H, Ar-H), 7.71 (d, 1H, *J* = 8.10 Hz, Ar-H), 7.78 (dd, 1H, *J* = 7.05 Hz, 1.15 Hz, Ar-H), 8.04–8.09 (m, 2H, Ar-H), 8.29–8.31 (m, 1H, Ar-H); ^{13}C NMR (125 MHz, DMSO-d_6) δ 107.82, 112.95, 120.07, 122.73, 124.23, 125.74, 125.90, 126.64, 127.24, 127.68, 128.92, 130.19, 130.47, 133.89, 135.27, 136.80, 144.15, 149.91, 157.11, 164.14, 168.33; MS (ESI+) *m/z* 338.56. Anal. Calcd for $C_{21}H_{15}N_5$: C, 74.76; H, 4.48; N, 20.76. Found: C, 75.11; H, 4.82; N, 20.99.

4-(1*H*-Benzimidazol-2-yl)-6-(4-bromophenyl)pyrimidin-2-amine (3d)

Yield 24%; mp 102 °C. ^{1}H NMR (500 MHz, DMSO-d_6) δ 6.87 (brs, 2H, NH2), 7.26–7.30 (m, 2H, Ar-H), 7.60–7.61 (m, 2H, Ar-H), 7.75 (d, 2H, *Jo* = 8.5 Hz, Ar-H), 7.97 (s, 1H, pyrimidine H-5), 8.15 (d, 2H, *Jo* = 8.5 Hz, Ar-H), 13.3 (s, 1H, NH); ^{13}C NMR (125 MHz, DMSO-d_6) δ 102.88, 112.97, 120.05, 122.78, 124.25, 124.91, 129.37, 131.56, 132.29, 135.25, 136.45, 144.17, 149.93, 157.87,

164.29, 164.39, 172.49; MS (ESI+) *m/z* 366.51 (M+H), 368.51 (M+H+2). Anal. Calcd for $C_{17}H_{12}BrN_5$: C, 55.75; H, 3.30; N, 19.12. Found: C, 56.18; H, 3.74; N, 19.50.

4-(1*H*-Benzimidazol-2-yl)-6-phenylpyrimidin-2-amine (3e)

Yield 17%; mp 172 °C (lit.[24] 192–194 °C). ^{1}H NMR (500 MHz, DMSO-d_6) δ 6.95 (brs, 2H, NH_2), 7.20 (brs, 1H), 7.35–7.36 (m, 2H, Ar-H), 7.56–7.59 (m, 2H, Ar-H), 7.72–7.74 (m, 3H, Ar-H), 8.16 (s, 1H, Ar-H), 8.21–8.23 (m, 2H, Ar-H); ^{13}C NMR (100 MHz, DMSO-d_6) δ 104.47, 116.18, 124.32, 127.08, 127.37, 129.34, 129.51, 131.50, 136.93, 149.23, 152.20, 156.00, 158.76, 164.12, 165.85; MS (ESI+) *m/z* 288.5 (M+H). Anal. Calcd for $C_{17}H_{13}N_5$: C, 71.06; H, 4.56; N, 24.37. Found: C, 69.59; H, 4.82; N, 24.80.

4-(1*H*-Benzimidazol-2-yl)-6-(2-fluorophenyl)pyrimidin-2-amine (3f)

Yield 15%; mp 121 °C. ^{1}H NMR (500 MHz, DMSO-d_6) δ 6.88 (brs, 2H, NH_2), 7.23–7.31 (m, 2H, Ar-H), 7.38–7.42 (m, 2H, Ar-H), 7.57–7.76 (m, 2H, Ar-H), 7.75 (d, 1H, *Jo* = 7.95 Hz, Ar-H), 7.87 (d, 1H, *J* = 2.45 Hz, Ar-H), 8.09 (tdd, 1H, *J* = 7.9 Hz, 7.8 Hz, 1.8 Hz, 1.75 Hz, Ar-H), 13.04 (s, 1H, NH); ^{13}C NMR (125 MHz, DMSO-d_6) δ 106.85–106.93 (d, *J* = 10.27 Hz), 112.95, 116.93–117.12 (d, *J* = 22.58 Hz), 120.12, 122.74, 124.26, 125.29–125.31 (d, *J* = 2.98 Hz), 125.51–125.60 (d, *J* = 10.66 Hz), 130.87, 132.85–132.92 (d, *J* = 8.77 Hz), 135.27, 144.14, 149.80, 157.48, 160.09, 161.95–162.08 (d, *J* = 16 Hz), 164.24; MS (ESI+) *m/z* 306.5 (M+H). Anal. Calcd for $C_{17}H_{12}FN_5$: C, 66.88; H, 3.96; N, 22.94. Found: C, 66.39; H, 3.74; N, 23.26.

4-(1*H*-Benzimidazol-2-yl)-6-[4-(benzyloxy)phenyl]pyrimidin-2-amine (3g)

Yield 10%; mp 240 °C. ^{1}H NMR (500 MHz, DMSO-d_6) δ 5.24 (2, 2H, CH_2), 6.72 (brs, 2H, NH_2), 7.15–7.50 (m, 9H, Ar-H), 7.60 (d, 1H, *J* = 7.80 Hz, Ar-H), 7.75 (d, 1H, *J* = 7.85 Hz, Ar-H), 7.91 (s, 1H, pyrimidine H-5), 8.17 (d, 2H, *J* = 8.80 Hz, Ar-H); ^{13}C NMR (125 MHz, DMSO-d_6) δ 69.87, 102.26, 112.90, 114.77, 115.47, 119.98, 122.67, 124.11, 128.26, 128.42, 128.96, 129.76, 131.37, 135.21, 137.24, 144.14, 150.17, 157.33, 161.09, 164.20, 165.04; MS (ESI+) *m/z* 394.7 (M+H). Anal. Calcd for $C_{24}H_{19}N_5O$: C, 73.27; H, 4.87; N, 17.80. Found: C, 73.61; H, 4.45; N, 18.09.

4-(1*H*-Benzimidazol-2-yl)-6-(thiophen-2-yl)pyrimidin-2-amine (3h)

Yield 13%; mp 118 °C. ^{1}H NMR (400 MHz, DMSO-d_6) δ 6.77 (brs, 2H, NH_2), 7.21–7.26 (m, 3H, Ar-H), 7.60 (brs, 1H, Ar-H), 7.71 (brs, 1H, Ar-H), 7.78 (dd, 1H, *J* = 4 Hz, 1.2 Hz, thiophene-H), 7.87 (s, 1H, pyrimidine H-5), 8.05 (dd, 1H, *J* = 4 Hz, 1.2 Hz, thiophen-H), 13.00 (brs, 1H, NH); ^{13}C NMR (100 MHz, DMSO-d_6) δ 101.45, 112.94, 120.02, 122.74, 124.23, 128.69, 129.18, 130.86, 135.19, 143.01, 144.10, 149.89, 157.29, 160.67, 163.93; MS (ESI+) *m/z* 294.47 (M+H), 296.27 (M+H+2). Anal. Calcd for $C_{15}H_{11}N_5S$: C, 61.42; H, 3.78; N, 23.87; S, 10.93. Found: C, 61.20; H, 3.39; N, 24.15; S, 10.58.

2. 2. Antimicrobial Activity Tests

In the antibacterial activity tests, *Staphylococcus aureus* ATCC 29213 (methicillin-susceptible, MSSA), *Staphylococcus aureus* ATCC 43300 (methicillin-resistant, MRSA), *Escherichia coli* ATCC 25922, and *Pseudomonas aeruginosa* ATCC 27853 were used as test bacteria. For the determination of minimum inhibitory concentration (MIC) values, the broth microdilution method was used.[26] Serial two-fold dilutions ranging from 512 μg/mL to 4 μg/mL were prepared in Mueller-Hinton Broth (Difco, Difco Laboratories, Detroit, MI, USA). The inoculums were prepared from subcultures for 24 h. The final test concentration of the bacteria was adjusted to 5×10^5 cfu/mL. The microplates were incubated at 35 °C for 18–24 h. The last well that completely inhibited visual microbial growth was noted as the MIC value (μg/mL).

The antifungal activity of the compounds was also evaluated by the determination of the MIC values (μg/mL). *Candida albicans* ATCC 10231 was used as the test organism. Serial two-fold dilutions ranging from 512 μg/mL to 4 μg/mL were prepared in RPMI 1640 broth (ICN-Flow, Aurora, OH, USA, with glutamine, without bicarbonate, and with pH indicator). The final test concentration of the fungus was 0.5 to 2.5×10^3 cfu/mL. The microplates were incubated at 35 °C for 48 h. The last well that completely inhibited visual microbial growth was noted as the MIC value (μg/mL). [27]

Test compounds were dissolved in dimethyl sulfoxide (DMSO; Sigma, USA) and 10% DMSO was used as the negative control. Ciprofloxacin (Sigma, USA) and gentamicin (Sigma, USA), fluconazole (Sigma, USA) were used as reference drugs.[28] Each experiment was performed in triplicate.

2. 3. Molecular Docking

Molecular docking studies were performed using the Maestro module of Schrödinger software 2021.2 version. Protein preparation was done with the 'Protein Preparation Wizard' module. FabH and CYP51 target proteins were prepared to add H atoms, creating disulfide bonds and removing waters and other heteroatoms. H bonds assignment for protein optimization according to sample water orientations with PROPKA pH:7.0 was performed. The protein minimization stage was performed with converging heavy atoms to RMSD:0.3 Å and OPLS4[28] force field. Ligand 3D minimized structures were prepared using OPLS4 force field in pH 7±2 with the 'LigPrep' module. The active site was determined according to the native ligands of target proteins, and the 20·20·20 $Å^3$ area was created by the 'Receptor Grid Generation' module. Molecular

docking was carried out using the 'Glide XP'[29] module, and Molecular Mechanics Generalized Born Surface Area (MM-GBSA) dG bind (binding free energy, kcal/mol) was measured using Prime module of Schrödinger software. 2D protein-ligand interactions and 3D binding mode analysis were performed with Chimera v.1.15, and Discovery Studio Visualizer v2021.

2. 4. Molecular Dynamics

Molecular dynamics simulation was performed with Gromacs 2019.2 version (GROningen MAchine for Chemical Simulations) to investigate the FabH·**3a** and the FabH·**3b** complex's protein-ligand stability. The **3a** and **3b** compounds structure's topology was created by the GlycoBioChem PRODRG2 server, the topology file of the FabH enzyme was created with the GROMOS 43a1 force field [31,32] and SCP water model. The energy of the formed protein, ligand, ion, and solvent system was minimized in 5000 steps with the steepest descent integrator algorithm. The system was balanced with 0.3 ns NVT and 0.3 ns NPT stages at 1 atm pressure and 300 K temperature according to the V-rescale[32] thermostat and Parrinello-Rahman[34] barostat. The 100 ns molecular dynamics simulation was performed with leap-frog MD integrator. Trajectory analysis was performed with gmx scripts, the root mean square deviation (RMSD) and the root mean square fluctuation (RMSF) measurements were performed. MD trajectory analysis results were monitored with VMD-Visual Molecular Dynamics v.1.9.3, BIOVIA Discovery Studio Visualizer v.2021, and graphs were generated with GraphPad Prism v.8.0.1. The binding free energy calculation by molecular mechanics Poisson–Boltzmann surface area (MM-PBSA) was performed between 80 and 100 ns using RashmiKumari's g_mmpbsa package.[35–37] The average binding free energy was calculated by using the 'MmPbSaStat' Python script provided in g_mmpbsa.

2. 5. ADME Predictions

The theoretical ADME parameters of the selected compounds were calculated with the Schrödinger software 'QikProp' module. Molecular weight, QPlogPo/w, QPlogHERG, QPPCaco, QPlogBB, QPPMDCK, percentage human oral absorption, rule of five, and rule of three were calculated.

3. Results

3. 1. Chemistry

Novel 1-(1*H*-benzimidazol-2-yl)-3-aryl-prop-2-en-1-ones and 4-(1*H*-benzimidazol-2-yl)-6-arylpyrimidin-2-amine derivatives were synthesized as described in Scheme 1. 2-Acetylbenzimidazole (**1**) was prepared by condensation of *o*-phenylenediamine and lactic acid[22–24] and followed by oxidation with potassium dichromate in the presence of sulfuric acid.[23–24]

The arylidene derivatives **2a**–**h** were synthesized *via* Claisen–Schmidt condensation of 2-acetyl benzimidazole (**1**) with aromatic aldehydes in ethanol at room temperature, the reaction was catalyzed by potassium hydroxide solution.[25] Although two types of geometric isomers could

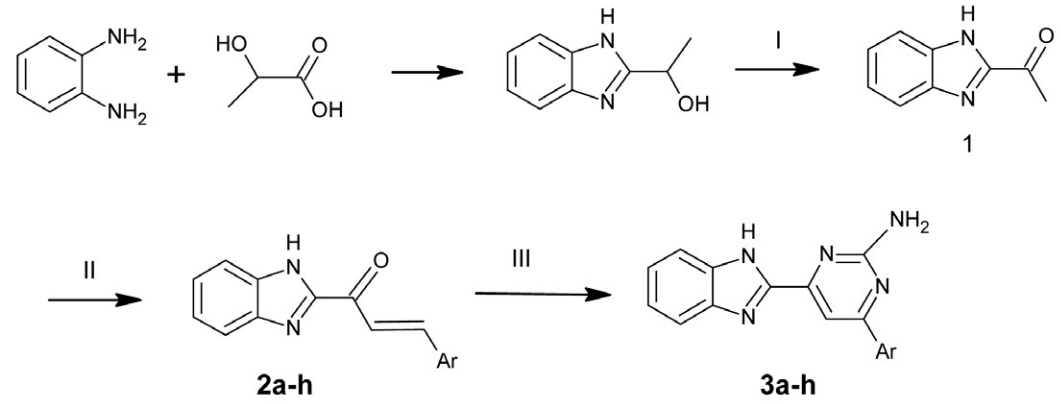

Reagents: (I) $K_2Cr_2O_7/H_2SO_4$; (II) ArCHO/EtOH; (III) guanidin HCl/NaH

		Ar
2a	**3a**	4-fluoro-3-bromophenyl
2b	**3b**	2-naphtyl
2c	**3c**	1-naphtyl
2d	**3d**	4-bromophenyl
2e	**3e**	phenyl
2f	**3f**	2-fluorophenyl
2g	**3g**	4-benzyloxyphenyl
2h	**3h**	2-thienyl

Scheme 1. Synthesis of compounds **2** and **3**

be expected for compounds **2a**–**h**, only (*E*) isomers were obtained. This is demonstrated by the ^{1}H NMR spectra, supported by the appearance of characteristic *trans*-coupling constants belonging to the aryldene protons in the range of 15.85–16.4 Hz.

The reaction of compounds **2a**–**h** with guanidine hydrochloride in the presence of NaH[25] was conducted to give the respective 4-(1*H*-benzimidazol-2-yl)-6-(aryl)pyrimidin-2-amines **3a**–**h**.

3. 2. Antimicrobial Activity

All the synthesized compounds **2** and **3** were evaluated for their antimicrobial activities *in vitro* against *Staphylococcus aureus* (ATCC 29213-methicillin-susceptible, MSSA, and ATCC 43300-methicillin-resistant, MRSA) as gram-positive, two gram-negative (*Escherichia coli* ATCC 25922, and *Pseudomonas aeruginosa* ATCC 27853) bacteria, and *Candida albicans* ATCC 10231 as fungus using the standard two-folds serial dilution method in 96-well micro-test plates recommended by the National Committee for Clinical and Laboratory Standards Institute.[26,27] Minimal inhibitory concentration (MIC, μg/mL) was defined as the lowest concentration of new compounds that completely inhibited the growth of bacteria and fungus. Ciprofloxacin, gentamicin, and fluconazole were used as the reference drugs.[28]

The antimicrobial results *in vitro* (Table 1) revealed that most of the prepared compounds could effectively inhibit the growth of some tested strains and that gram-positive bacteria are more sensitive to the tested compounds than the gram-negative bacteria and fungus. Moreover, in most of the compounds, amino pyrimidines were observed to be more active than the arylidene counterparts.

Regarding the activity of individual compounds, it is noteworthy that bearing 4-fluoro-3-bromophenyl (**3a**) and 2-naphthyl (**3b**) as aryl group at the position 4 of pyrimidine ring are the most active analogs; they exhibited <4 μg/mL MIC values against both *S. aureus*. **2f** (Ar = 2-fluorophenyl), **3e** (Ar = phenyl), and **3h** (Ar = thienyl) also displayed moderate to good activities against the gram-positive bacterial strains. In addition, compounds **2f** and **3h** showed moderate antifungal efficacy toward *C. albicans* with 16 μg/mL MIC values. The rest of the investigating benzimidazoles exerted either weaker activity or were totally inactive toward the tested microbial strains.

3. 3. Computational Studies

3. 3. 1. Molecular Docking Analysis

Molecular docking studies are computational methods frequently used in drug design to predict how small molecule compounds interact with target macromolecules at the atomic level.[38–40] In this study, molecular docking analyses of compounds with MIC values of 16 μg/mL and below against gram-positive bacteria and fungi were performed. FabH (β-ketoacyl-acyl carrier protein synthase III) was preferred as the bacterial target protein and CYP51 (sterol 14α-demethylase) was preferred as the fungal target protein. To validate the molecular docking process, the natural ligand re-docking process in the crystal structures of the target enzymes was performed. Ligand and protein

Table 1. MIC values (μg/mL) of the synthesized compounds

Compound	Gram-positive bacteria		Gram-negative bacteria		Fungus
	S. aureus ATCC 29213 (MSSA)	*S. aureus* ATCC 43300 (MRSA)	*E. coli* ATCC 25922	*P. aeruginosa* ATCC 27853	*C. albicans* ATCC 10231
2a	64	64	256	128	–
2b	128	128	–	–	128
2c	64	64	–	128	128
2d	64	64	–	–	–
2e	128	128	256	128	64
2f	16	16	256	256	16
2g	64	64	–	–	–
2h	128	128	256	256	128
3a	<4	<4	256	256	–
3b	<4	<4	256	256	64
3c	32	64	256	256	128
3d	64	128	–	128	128
3e	16	16	256	128	64
3f	32	64	256	256	64
3g	64	128	–	–	128
3h	16	16	256	256	16
Ciprofloxacin	<0.25	0.5	<0.25	<0.25	NT
Gentamicin	0.5	<0.25	0.5	<0.25	NT
Fluconazole	NT	NT	NT	NT	1.56

NT: Not tested **"–": represents no activity**

Table 2. Glide XP molecular docking, prime binding free energy and protein-ligand interactions results performed against bacterial (FabH) and fungal (CYP51) target enzymes

Target enzymes	Comp.	XP GScore	MMGBSA dG Bind	Protein-ligand interactions
FabH (PDB ID: 3IL5)	**2f**	–8.75	–60.11	**Asn253** (2.50 Å), **Asn280** (2.80 Å, 1.96 Å), Asn280, Phe312, Ile223, Ala227, Ala252, Ile223, Ala252
	3a	–8.50	–65.52	**Ala252** (2.06 Å), Gly313, Phe312, Cys117, Leu194, His250, Arg221, Ala252, Ile223, Ala227, Ala252
	3b	–7.90	–60.64	Cys117, His250, Phe224, Arg221, Ile223, Ala252, Ile256, Leu194, Ile223, Ala252
	3e	–8.33	–56.69	**Gly220** (2.51 Å), **Ala252** (1.97 Å), Met218, Phe312, Ala252, Ile223, Ala227, Ala252
	3h	–7.51	–61.75	**Gly220** (2.42 Å), **Ala252** (2.24 Å), Ala252, Met218, Phe312, Ile223, Ile223, Ala227, Ala252
CYP51 (PDB ID: 5TZ1)	**2f**	–7.97	–47.97	Phe380, Phe233, Leu376, Leu376, Ile131, Hem601
	3h	–7.07	–47.94	**Met508** (3.69 Å), Tyr118, Tyr118, His377, Pro230, Pro230, Met508, Leu121, Leu376, Met508, Leu376, Met508

FabH: β-ketoacyl-acyl carrier protein synthase III (PDB ID: 3IL5), CYP51: sterol 14α-demethylase, XP Gscore (kcal/mol): Extra Precision Glide Score, MMGBSA dG Bind (kcal/mol): Molecular Mechanics Generalized Born Surface Area total binding energy.

structures were minimized using the OPLS4 force field. As given in Table 2, Glide XP binding energies were below –7 kcal/mol and MMGBSA binding free energy values were below –47 kcal/mol. Again, in Table 2, the protein–ligand interaction details of the selected compounds are explained.

The binding poses and schematic protein-ligand interactions of the two most active compounds, **3a** and **3b**, at the FabH active site are shown in Figure 1. Compound **3a** showed H bond between –NH group of 2-aminopyrimidine structure and Ala252, hydrophobic interactions with Gly313, Phe312, Cys117, Leu194, His250, Arg221, Ala252, Ile223, and Ala227. Compound **3b**, on the other hand, formed hydrophobic interactions with Cys117, His250, Phe224, Arg221, Ile223, Ala252, Ile256, Leu194, and Ile223, although there was no H bond formation.

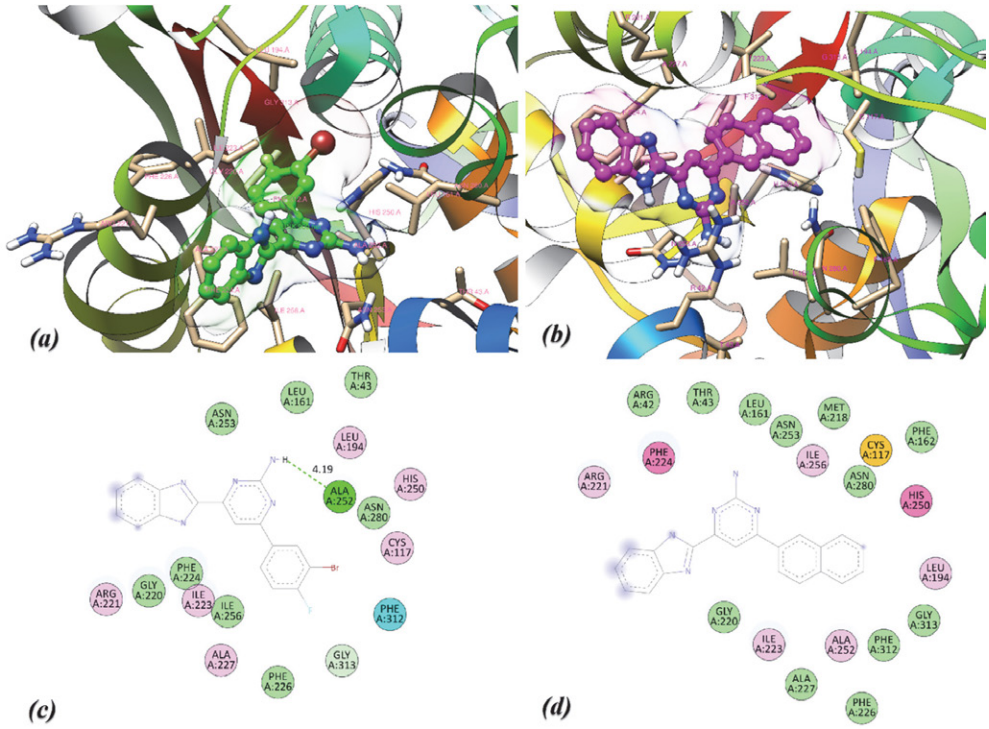

Figure 1. Visualization of the results from the Glide XP molecular docking study performed against bacterial target enzyme FabH. (**a**) Binding pose of compound **3a** and (**b**) compound **3b**, and 2D schematic protein-ligand interactions of (**c**) compound **3a** and (**d**) compound **3b**

3. 3. 2. Molecular Dynamics Simulations

Molecular dynamics simulations are widely used to study the stability of protein-ligand complexes obtained from molecular docking.[37,40,41] By modeling the protein-ligand complex *in silico* physiological conditions, the variation and stability of the protein-ligand interaction can be predicted. Accordingly, the protein-ligand interaction of FabH·**3a** and FabH·**3b** complexes obtained from the Glide XP molecular docking study was investigated for the two most active compounds. 100 ns molecular dynamics simulation was performed, RMSD and RMSF trajectory analyzes were performed. RMSD is one of the most basic parameters used to analyze aberrations in protein structure. As seen in Figure 2, after the first 20 ns, just above 0.4 nm, the deviations continue to be stable at a minor level after the system stabilizes. The mean RMSD value of the FabH·**3a** and FabH·**3b** complex was measured as 0.44 nm and 0.41, respectively. RMSF is another analysis parameter that provides information on protein fluctuations and conformational changes. As seen in Figure 2, some different fluctuations occurred with the binding of **3a** and **3b** with FabH. The lower RMSF value than **3b** was measured around the Ser41 residues, where **3a** gave H-bond interaction. This H bond reduced protein mobility and made it more stable. **3b**, on the other hand, formed strong hydrophobic interactions with Phe312, significantly reducing FabH mobility.

To examine the protein-ligand interaction and binding pose during the molecular dynamics simulation of compound **3a**, its changes in the middle and at the end of the 100 ns simulation were analyzed. As shown in Figure 3, compound **3a** remained stable at the active site. The H bond and basic hydrophobic interactions between –NH of the benzimidazole core and Ser41 were preserved.

Measuring the binding free energy between protein and ligand in molecular dynamics simulations is another important approach. MMPBSA is obtained by summing the averages of Van der Waals, electrostatic, polar solvation, and solvent accessible surface area (SASA) energies. In this study, the average binding free energy of **3a** and **3b** compounds with FabH was calculated between 80 ns and

Table 3. MM-PBSA binding free energies of FabH with compounds **3a** and **3b** between 80 ns and 100 ns.

Parameters (Energy)	Enzyme-ligand complexes FabH · 3a (kJ/mol)	FabH · 3b (kJ/mol)
Van der Waals	–207.305 ± 12.271	–272.200 ± 10.109
Electrostatic	3.695 ± 3.356	1.563 ± 2.200
Polar solvation	41.219 ± 13.297	45.524 ± 6.006
SASA	–18.603 ± 10.999	–20.690 ± 0.835
Binding free	**–180.993 ± 15.364**	**–245.803 ± 10.893**

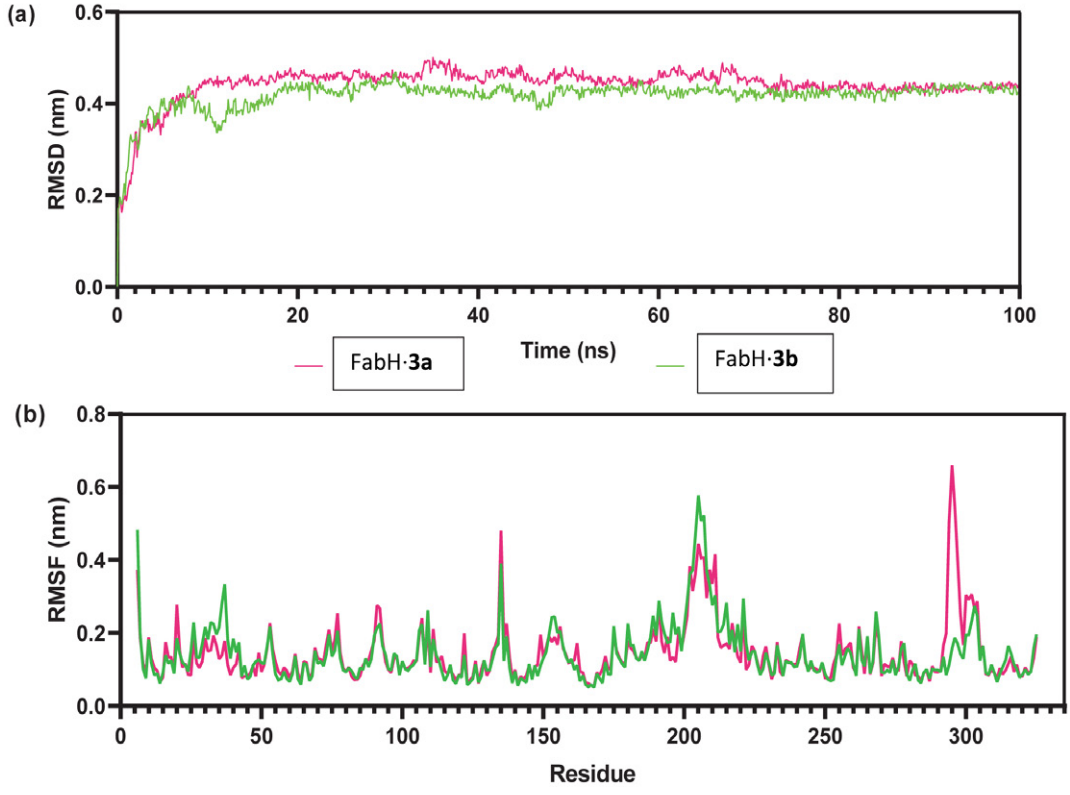

Figure 2. Molecular dynamics simulation trajectory analysis of **3a** and **3b** with FabH enzyme throughout 100 ns (**a**) RMSD of ligand-bound FabH·**3a** (magenta) and FabH·**3b** (green), (**b**) RMS fluctuation values during the period of simulation

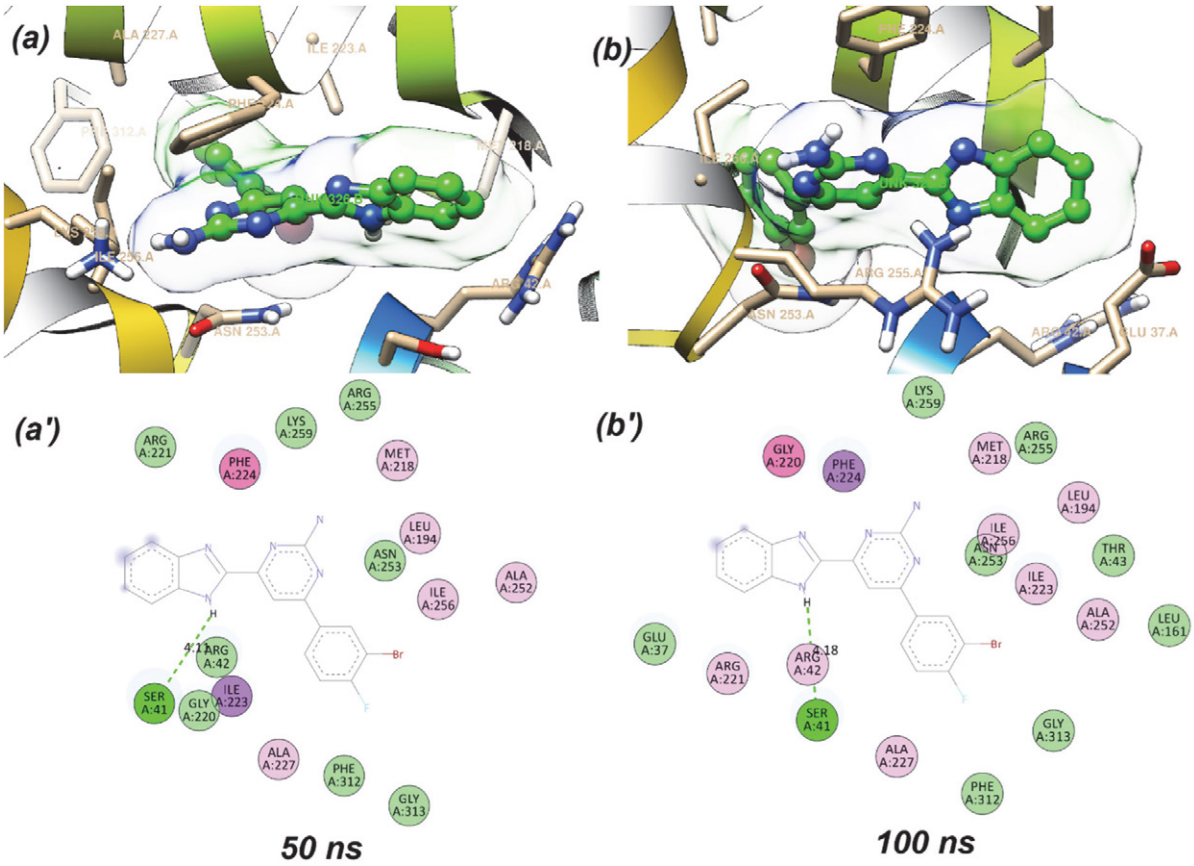

Figure 3. Binding pose and protein-ligand schematic interactions of compound **3a** in the FabH active site (**a**, **a'**) in the middle (50 ns), (**b**, **b'**) and at the end (100 ns) of the molecular dynamics simulations.

100 ns. The average of –180.993 kJ/mol and –245.883 kJ/mol binding free energy was found between **3a** and **3b** compounds and FabH, respectively. Interactions energy details are given in Table 3.

3. 3. 3. ADME Estimations

Drug discovery is a long, expensive and risky process that includes drug candidate identification, candidate validation, pharmacokinetics, and preclinical toxicity assessment studies. *In silico*, drug discovery technology plays an important role in the pharmaceutical industry. One of these technologies is *in silico* ADME prediction. ADME parameters, together with the drug discovery process, contribute to the selection of the therapeutic dose and identification of molecules with the optimal safety profile. Early prediction of ADME parameters has been shown to significantly reduce the pharmacokinetics failure rate at clinical stages during the discovery phase and avoid wasting time and resources in the discovery of drug molecules.[43] ROF value Lipinski's rule of five, also known as Pfizer's five rules or only the five rules (ROF), is a rule of thumb for assessing drug similarity or determining whether a chemical compound with a particular pharmacological or biological activity has favorable chemical and physical properties. According to this rule, the ligand molecule should have no more than 5 hydrogen bond donors, no more than 500 molecular weight, no more than 5 log *P*, and no more than 10 N and O atoms.[44] ROT value should be greater than the estimated aqueous solubility (logS) –5.7, predicted apparent Caco-2 cell permeability (PCaco) greater than 22 nm/s, and primary metabolites (PM) less than 7 according to Jorgensen's rule of three. The QPlogPo/w value is the estimated octanol/water coefficient and should be in the range of –2.0 to 6.5. QPlogHERG is the estimated IC_{50} for blocking HERG K^+ channels below –5 is of concern. QPPCaco Estimated apparent Caco-2 cell permeability in nm/second Caco-2 cells are a model for the intestinal blood barrier. QikProp estimates are for inactive transport. Values below 25 are weak, above 500 are great. QPlogBB is the estimated brain/blood partition coefficient and should has a value between –3.0 and 1.2. QPPMDCK Estimated apparent MDCK cell permeability in nm/s. MDCK cells are considered a good mimic of the blood-brain barrier. QikProp estimates are for inactive transport. Percent Human Oral Absorption (PHOA) is estimated human oral absorption on a scale of 0% to 100%. Values above 80% are great, below 20% are weak. For this pur-

Table 4. ADME parameters data of selected compounds

Compounds	MW	QPlogPo/w	QPlogHERG	QPPCaco	QPlogBB	QPPMDCK	PHOA	ROF	ROT
2f	266.2	3.287	–6.0	1483.2	–0.411	1226.717	100.0	0	0
3a	384.2	3.507	–6.2	652.5	–0.531	1330.029	100.0	0	0
3b	337.3	3.677	–7.0	639.4	–0.845	305.129	100.0	0	0
3e	287.3	2.752	–6.4	643.1	–0.780	307.012	93.3	0	0
3h	293.3	2.672	–6.0	637.6	–0.599	529.965	92.7	0	0

pose, some important physicochemical properties, and descriptors of **2f**, **3a**, **3b**, **3e**, and **3h** were calculated theoretically using Schrödinger Maestro's QikProp module and are presented in Table 4. According to Lipinski's five rules and Jorgensen's three rules in these calculations, drug candidates should not have more than one violation in their ADME profile. All compounds in the table appear to comply with these rules.

These results increase the possibility that the compounds are potential drug molecules, given the promising antimicrobial activity results.

4. Conclusion

Results from molecular docking and molecular dynamics simulation studies show that active compounds **3a** and **3b** form strong interactions at the FabH active site. According to the molecular docking analysis, it was calculated that sufficient protein-ligand interaction energy was formed between the compounds **2f**, **3a**, **3b**, **3e**, and **3h** and the antibacterial target protein FabH, and strong interactions were formed between the compounds **2f** and **3h** and the antifungal target protein. It is understood that compounds **3a** and **3b** with MIC values below 4 μg/mL maintain protein-ligand stability *in silico* physiological conditions, according to RMSD, RMSF, and MMPBSA measurements obtained from molecular dynamics.

Conflicts of Interests

The authors declare that there are no conflicts of interests.

Acknowledgement

The authors thank to Ankara University-Scientific Research Unit supplying the Schrödinger software program purchased under grant project number BAP-21B0237004.

All molecular dynamics simulations reported were performed utilizing TÜBİTAK (The Scientifc and Technological Research Council of Turkey), ULAKBİM (The Turkish Academic Network and Information Center), and the High Performance and Grid Computing Center (TRUBA resources).

5. References

1. R. Srivastava, S. K. Gupta, F. Naaz, A. Singh, V. K. Singh, R. Verma, N. Singh, R. K. Singh, *Comput. Biol. Chem*. **2018,** *76*, 1–16. **DOI:**10.1016/j.compbiolchem.2018.05.021
2. M. Abdel-Motaal, K. Almohawes, M. A. Tantawy, *Bioorg. Chem*. **2020**, *101*, 103972. **DOI:**10.1016/j.bioorg.2020.103972
3. S. Malasala, N. Ahmad, R. Akunuri, M. Shukla, G. Kaul, A. Dasgupta, Y. V. Madhavi, S. Chopra, S. Nanduri, *Eur. J. Med. Chem*. **2021**, *212*, 112996. **DOI:**10.1016/j.ejmech.2020.112996
4. E. M. E. Dokla, N. S. Abutaleb, S. N. Milik, D. Li, K. El-Baz, M. W. Shalaby, R. Al-Karaki, M. Nasr, C. D. Klein, K. A. M. Abouzid, M. N. Seleem, *Eur. J. Med. Chem*. **2020**, *186*, 111850. **DOI:**10.1016/j.ejmech.2019.111850
5. H. Chaurasia, V. K. Singh, R. Mishra, A. K. Yadav, N. K. Ram, P. Singh, R. K. Singh, *Bioorg. Chem*. **2021**, *115*, 105227. **DOI:**10.1016/j.bioorg.2021.105227
6. C. Sun, S. Zhang, P. Qian, Y. Li, H. Deng, W. Ren, L. Jiang, *Bioorg. Med. Chem. Lett.* **2021**, *47*, 128210. **DOI:**10.1016/j.bmcl.2021.128210
7. I. Kerimov, G. Ayhan-Kilcigil, E. D. Ozdamar, B. Can-Eke, T. Coban, S. Ozbey, C. Kazak, *Arch. Pharm.* **2012**, *345(7)*, 549–556. **DOI:**10.1002/ardp.201100440
8. A. S. Alp, G. Kilcigil, E. D. Özdamar, T. Çoban, B. Eke, *Turk. J. Chem*. 2015, *39(1)*, 42–53. **DOI:**10.3906/kim-1403-44
9. G. Ayhan-Kilcigil, C. Kus, T. Coban, E. D. Ozdamar, B. Can-Eke, *Arch. Pharm.* 2014, *347(4)*, 276–282. **DOI:**10.1002/ardp.201300324
10. R. Sireesha, R. Sreenivasulu, C. Chandrasekhar, S. S. Jadav, Y. Pavani, M. V. B. Rao, M. Subbarao, *J. Mol. Struct*. **2021**, *1226*, Part B, 129351. **DOI:**10.1016/j.molstruc.2020.129351
11. M. T. E. Maghraby, O. M. F. Abou-Ghadir, S. G. Abdel-Moty, A. Y. Ali, O. I. A. Salem, *Bioorg. Med. Chem*. **2020**, *28(7)*, 115403. **DOI:**10.1016/j.bmc.2020.115403
12. F. Doganc, I. Celik, G. Eren, M. Kaiser, R. Brun, H. Goker, *Eur. J. Med. Chem*. **2021**, *221*, 113545. **DOI:**10.1016/j.ejmech.2021.113545
13. M. Bessières, E. Plebanek, P. Chatterjee, P. Shrivastava-Ranjan, M. Flint, C. F. Spiropoulou, D. Warszycki, A. J. Bojarski, V. Roy, L. A. Agrofoglio, *Eur. J. Med. Chem*. **2021**, *214*, 113211. **DOI:**10.1016/j.ejmech.2021.113211
14. S. Hussain, M. Taha, F. Rahim, S. Hayat, K. Zaman, N. Iqbal, M. Selvaraj, M. Sajid, M. A. Bangesh, F. Khan, K. M. Khan, N. Uddin, S. A. A. Shah, M. Ali, *J. Mol. Struct*. **2021**, *1232*, 130029. **DOI:**10.1016/j.molstruc.2021.130029
15. Z. Wu, M. B. Xia, D. Bertsetseg, Y. H. Wang, X. L. Bao, W. B.

Zhu, T. Xu, P. R. Chen, H. S. Tang, Y. J. Yan, Z..L. Chen, *Bioorg. Chem*. **2020**, *101*, 104042. **DOI:**10.1016/j.bioorg.2020.104042
16. M. M. Sirim, V. S. Krishna, D. Sriram, O. Unsal Tan, *Eur. J. Med. Chem*. **2020**, *188*, 112010. **DOI:**10.1016/j.ejmech.2019.112010
17. T. Zhang, Q. Liu, Y. Ren, *Tetrahedron* **2020**, *76(13)*, 131027. **DOI:**10.1016/j.tet.2020.131027
18. S. Sana, V. G. Reddy, T. S. Reddy, R. Tokala, R. Kumar, S. K. Bhargava, N. Shankaraiah, *Bioorg. Chem*. **2021**, *110*, 104765. **DOI:**10.1016/j.bioorg.2021.104765
19. V. Rastija, D. Agić, S. Tomić, S. Nikolić, M. Hranjec, G. Karminski-Zamola, M. Abramić, *Acta Chim. Slov*. **2015**, *62*, 867–878. **DOI:**10.17344/acsi.2015.1605
20. I. Celik, G. Ayhan-Kilcigil, B. Guven, Z. Kara, S. Gurkan-Alp, A. Karayel, A. Onay-Besikci, *Eur. J. Med. Chem*. **2019**, *173*, 240–249. **DOI:**10.1016/j.ejmech.2019.04.012
21. C. Kus, G. Ayhan-Kilcigil, S. Ozbey, F. B. Kaynak, M. Kaya, T. Coban, B. Can-Eke, B, *Bioorg. Med. Chem*. **2008**, *16(8)*, 4294–4303. **DOI:**10.1016/j.bmc.2008.02.077
22. M. Chandran, *J. Pharm. Res*. **2012**, *5(1)*, 324–326.
23. R. R. Kunduru, M. R. Vanga, S. Boche, *Int. J. Pharm. Sci. Invent.* **2014**, *3(6)*, 27–31.
24. R. R. Kunduru, M. R. Vanga, S. Boche, *Int. J. Pharm. Sci. Drug. Res.* **2014**, *6(4)*, 278–282.
25. H. B. Liu, W. W. Gao, V. K. R. Tangadanchu, C. H. Zhou, R. X. Geng, *Eur. J. Med. Chem*. **2018**, *143*, 66–84. **DOI:**10.1016/j.ejmech.2017.11.027
26. Clinical and Laboratory Standards Institute (CLSI). **2009**, Methods for dilution antimicrobial susceptibility tests for bacteria that grow aerobically. Approved standard. In: CLSI Publication M07-A8, 8th ed. Wayne, PA, USA.
27. Clinical and Laboratory Standards Institute (CLSI). **2008**, Reference method for broth dilution antifungal susceptibility testing of yeasts; approved standard. M27-A3, vol 29, 3rd ed., Wayne: PA, USA.
28. European Committee on Antimicrobial Susceptibility Testing. Breakpoint tables for interpretation of MICs and zone diameters. Version 3.1., valid from **2013**-02-11.
29. E. Harder, W. Damm, J. Maple, C. Wu, M. Reboul, J. Y. Xiang, R. A. Friesner, *J. Chem. Theory Comput*. **2016**, *12(1)*, 281–296. **DOI:**10.1021/acs.jctc.5b00864
30. E. P. Glide, *J Med Chem*. **2006**, *4*, 6177–6196.
31. M. J. Abraham, T. Murtola, R. Schulz, S. Páll, J. C. Smith, B. Hess, E. Lindahl, "GROMACS: High performance molecular simulations through multi-level parallelism from laptops to supercomputers," SoftwareX, **2015**, *1–2*, 19–25. **DOI:**10.1016/j.softx.2015.06.001
32. C. Oostenbrink, A. Villa, A. E. Mark, W. F. Van Gunsteren, *J. Comput. Chem.* **2004**, *25(13)*, 1656–1676. **DOI:**10.1002/jcc.20090
33. G. Bussi, D. Donadio, M. Parrinello, *J. Chem. Phys.* **2007**, *126(1)*, 014101. **DOI:**10.1063/1.2408420
34. M. Parrinello, A. Rahman, *J. Appl. Phys.* **1981**, *52(1)*, 7182–7190. **DOI:**10.1063/1.328693
35. R. Kumari, R. Kumar, Open Source Drug Discovery Consortium, A. Lynn, J. Chem. Inf. Model. **2014**, *54(7)*, 1951–1962. **DOI:**10.1021/ci500020m
36. N. A. Baker, D. Sept, S. Joseph, M. J. Holst, J. A. McCammon, Proc. Natl. Acad. Sci. **2001**, *98(18)*, 10037–10041. **DOI:**10.1073/pnas.181342398
37. N. Homeyer, H. Gohlke, *Mol. Inform.* **2012**, *31(2)*, 114–122. **DOI:**10.1002/minf.201100135
38. H. Ahmad, F. Ahmad, S. Parveen, S. Ahmad, S. S. Azam, A. Hassan, *Bioorg. Chem*. **2020**, *105*, 104426. **DOI:**10.1016/j.bioorg.2020.104426
39. Y. Huang, H. Hu, R. Yan, L. Lin, M. Song, X. Yao, *Arch. Pharm*. **2021**, *354(2)*, 2000165. **DOI:**10.1002/ardp.202000165
40. I. Celik, A. Onay-Besikci, G. Ayhan-Kilcigil, *J. Biomol. Struct. Dyn*. **2020**, *39(15)*, 5792–5798. **DOI:**10.1080/07391102.2020.1792993
41. K. N. Venugopala, M. Kandeel, M. Pillay, P. K. Deb, H. H. Abdallah, M. F. Mahomoodally, D. Chopra, *Antibiotics* **2020**, *9(9)*, 559. **DOI:**10.3390/antibiotics9090559
42. I. Celik, M. Erol, Z. Duzgun, *Mol. Divers.* **2021**, 1–14 **DOI:**10.1007/s11030-021-10215-5
43. L. L. Ferreira, A. D. Andricopulo, *Drug Discov. Today* **2019**, *24(5)*, 1157–1165. **DOI:**10.1016/j.drudis.2019.03.015
44. İ. Şahin, M. Çeşme, F. B. Özgeriş, F. Güngör, F. Tümer, *J. Mol. Struct.* **2022**, *1247*, 131344. **DOI:**10.1016/j.molstruc.2021.131344

Povzetek

Sintetizirali smo serijo novih derivatov benzimidazola ter določili njihove antimikrobne aktivnosti. Spojini **3a** in **3b** sta proti *Staphylococcus aureus* ATCC 29213 (MSSA) in *Staphylococcus aureus* ATCC 43300 (MRSA) pokazali odlično antibakterijsko aktivnost z MIC vrednostjo <4 μg/mL. Molekulsko sidranje spojin, ki so se proti gram-pozitivnim bakterijam in glivam izkazale z MIC vrednostmi 16 μg/mL in manj, smo izvedli z uporabo bakterijskega proteina FabH (β-ketoacil-acil protein sintaza III) oz. CYP51 (sterol 14α-demetilaza), ki je protein glive. Glede na rezultate molekulskega sidranja, smo ugotovili, da se pri interakciji proteina z ligandom sprosti dovolj energije v primerih, ko spojine **2f**, **3a**, **3b**, **3e** in **3h** interagirajo z antibakterijskim tarčnim proteinom FabH; močne so tudi interakcije v primeru, ko spojini **2f** in **3h** interagirata s tarčnim proteinom v primeru glive. Skladno z RMSD, RMSF in MMPBSA rezultati, dobljenimi z molekulsko dinamiko, izgleda, da spojini **3a** and **3b** ohranjata stabilno interakcijo proteina in liganda pod *in silico* fiziološkimi pogoji.